Northumbria
University
NEWCASTLE

Prediction of Machining Accuracy based on Geometric Error Estimation of Tool Rotation Profile in Five-axis Multi-layer Flank Milling Process

Hangzhuo Yu[1], Lei Jiang[1], Jindong Wang[1], Shengfeng Qin[2], Guofu Ding[1],

[1]Institute of Advanced Design and Manufacturing, School of Mechanical Engineering, Southwest Jiaotong University, Chengdu, China

[2]School of Design, Northumbria University, Newcastle upon Tyne, UK

Corresponding author:

Lei Jiang, Institute of Advanced Design and Manufacturing, School of Mechanical Engineering, Southwest Jiaotong University, Chengdu, 610031, China

E-mail: jianglei0506@163.com

Abstract： In a five-axis multi-layer flank milling process, the geometric error of a tool rotation profile caused by radial dimension error and setup error has a great influence on the machining accuracy. In this work, a new comprehensive error prediction model considering the inter-layer interference caused by tool rotation profile error is established, which incorporates a pre-existing prediction model dealing with a variety of errors such as geometric errors of machine tool, workpiece locating errors and spindle thermal deflection errors. Firstly, a series of tool contact points on the tool swept surface in each single layer without overlapping with others are calculated. Secondly, the position of the tool contact points on the overlapped layers is updated based on the detection and calculation of inter-layer interferences. Thirdly, all evaluated tool contact points on the final machined surface are available for completing the accuracy prediction of the machined surface. A machining experiment has been carried out to validate this prediction model and the results shows that this model is effective.

Keywords: Machining accuracy prediction, Tool rotation profile error, Multi-layer flank milling, Overlapping areas, Comprehensive error prediction model

1. Introduction

Flank milling is a common way of five-axis CNC machining, which provides line

contact between the tool profile and workpiece. When the tool moves along a predetermined trajectory relative to the workpiece, the machined surface is formed in the enveloping process in which the profile of tool rotation is projected on the surface perpendicular to the direction of feed motion or the tool path. This means that the contact line between the cutting tool and workpiece moves along the feed direction to generate a swept surface (an enveloping surface)[1-3], as shown in Fig. 1 and Fig. 5. Therefore, the tool path and the tool rotation profile have important influence on the machining surface[4-6]. The geometric errors of machine tool, workpiece locating errors, thermal deflection errors of machine axes will cause the deviation of tool location and tool orientation, which will lead to a tool path error[7-9]. The tool errors including radial dimensional error, setup error, wear and deflection will cause the geometric error of the rotation profile when the tool is rotating[5,10-14]. In order to manage the machining quality effectively, it is necessary to build a machining accuracy prediction model considering the influence of several main errors. Contact width between the tool and workpiece in flank milling is larger than that in ball-end milling, so the surface accuracy of the workpiece is more easily affected by the tool rotation profile, and the tool rotation profile error should be considered in the accuracy prediction model.

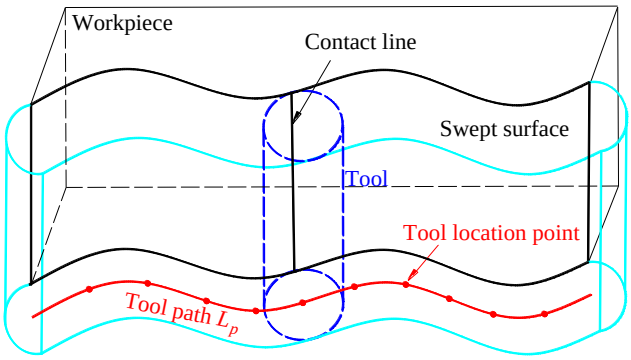

Fig. 1 Surface swept by tool contact line

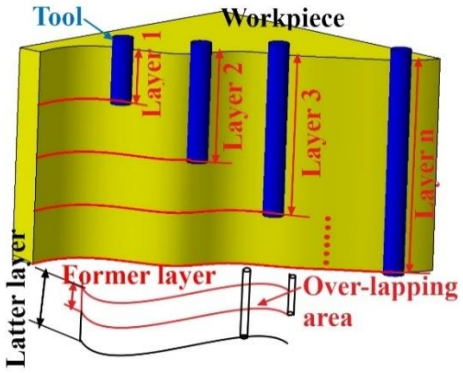

Fig. 2 Illustration of a multi-layer flank milling

As the machined surface is formed by sweeping the contact line, the profile of machined surface is closely related to the shape of the contact line. As shown in Fig. 1, if the actual contact line deviates from the ideal contact line due to tool rotation profile error, the actual sweep surface will deviate from the ideal sweep surface. In order to

describe the shape of the contact line, the contact line is discretized into a series of tool contact points[11]. Therefore, as long as the tool contact points on the machined surface are calculated, the surface machining accuracy can be evaluated.

As shown in Fig. 2, for stably flank milling a deep ruled surface, it may need multi-layer millings, each layer is machined at a different depth and two adjacent layers have some overlapping along the tool axial direction. As a result, the whole machined surface can be divided into several layers which distributed along the tool axial direction. The machining is carried out by the way of layer by layer, the swept surface is formed in each layer, and the overlap between former and latter layers. The tool sweeping in the latter layer may interfere with the swept surface on the former layer due to the geometric error of tool rotation profile, whereby affecting the machining accuracy[6,12]. Therefore, the influence of inter-layer interference needs to be considered in the accuracy prediction model.

Five-axis flank milling process involves many error factors. Many scholars have researched on the influence of various errors on the accuracy of machining and made a lot of research achievements. For tool cutting errors, due to the dimension error, setup error, deflection and wear, the influence of tool errors on machining surface quality cannot be ignored. For tool runout error, Ryu[15] et al. believed that tool runout error and setting error including tool tilting and eccentricity occurs when the tool axis does not coincide with the spindle axis, which results in the change of rotation radius along the axis, thus has a certain influence on surface topography. So Weinert[16] analyzed the effect of tool runout on surface by simulation of the dynamic milling process, and pointed out that the tool runout has a strong influence on tool vibration thus affect the surface topography. However, this method does not analyze the effect of runout parameters on surface morphology. Later, Arizmendi[14] established a surface topography prediction model for tool setting error by peripheral milling, and analyzed the effects of tool geometry and tool setting error parameters on the machined surface. On this basis, Guo[17], Kruger[18] and Artetxe[19] analyzed the effect of tool runout on surface topography by establishing several envelope models of tool runout in flank milling, these models realize the mapping between tool runout parameters and surface

accuracy. Fu[20] established an analytical force model considering tool runout, this model can analyze the influence of tool runout on milling force. Liu[21] and Sriyotha[22] analyzed the effects of tool runout and wear on machining accuracy. The aforementioned models introduce a series of runout parameters (such as offset vector, location angle, tilt angular position and so on), how to get these parameters accurately is very important. Wan[23] calculated the parameters from the average cutting force model, Qiang[24] proposed a new algorithm for determining runout parameters by establishing a cutting process geometry model to consider the tool runout and the runout parameters calculated by cutting forces model. But Kruger[18] pointed out that these parameters only can be deduced indirectly through the related milling force model because they are difficult to be calibrated by experiments, which will lead to some deviations.

Some authors studied the influence of the tool deflection and wear on machined surface. Zeroudi[25], Yuan[26], Islam[5] and Ko[27] et al. carried out the research on tool deflection error, several milling force models were established for end milling and flank milling respectively, the tool was regarded as a cantilever beam in a dynamic model of tool deflection and the influence of tool deflection on machining accuracy was analyzed. References [10,13,28-29] established several models about tool wear for ball-end milling and flank milling respectively to analyze the influence of tool wear on machining accuracy. It was pointed out that tool wear would affect milling force and coupling relationship with tool deflection, and it is difficult to obtain the milling force accurately in the process of machining. Therefore, it is difficult to analyze the effect of wear and deflection on machining accuracy separately by using theoretical models. For tool path errors, many scholars have established lots of prediction models using various error theories for carrying out machining accuracy prediction and error analysis. References [7,30-32] established several prediction models for geometric errors of machine tool based on multi-body system (MBS) theory and homogeneous transformation metrics technology. Zhang[33] and Jian[34] studied a dynamic spindle thermal error model including drift and tilt using MBS theory. Liu[35] developed a spindle radial thermal drift error model based on physical model. Kang[36] and Qin[37]

et al. investigated error models for workpiece positioning clamping based on Jacobi matrix method. On this basis, Khodaygan[38] developed a new matrix-based formulation to establish the relationship between the locating error and multiple error sources, and proposed a compensation method for workpiece locating error. These error models or analysis methods can be used to study the effects of individual errors on machining accuracy.

For comprehensive error modeling, Srivastava[39] and Zhang[40] established prediction models including geometric errors of machine tool and thermal errors based on MBS theory, but the prediction accuracy of thermal error needs to be improved. On this basis, Zhang[9] et al. proposed a comprehensive volumetric error model considering the geometric errors, thermal-induced errors and tool wear based on MBS and neural fuzzy control theory. Later, they optimized the total cost of machine tool by a geometric error budget method[41]. Liang[42] and Ramesh[43] studied a comprehensive error model including thermal error, geometric error and cutting force deflection error of machine tool, however, the prediction accuracy does not consider the influence of locating error. Therefore, Li[8] developed a comprehensive error model including locating error, spindle error, geometrical errors of the machine tool, and cutting tool deflection using MBS theory for five-axis ball-end milling, this model improves the prediction accuracy of tool path error. Yu[44] developed a prediction model considering the tool path errors and tool errors including tool dimension error, setup error, tool wear and deflection in flank milling. However, this model does not consider the influence of inter-layer interference and cannot be applied to multi-layer machining.

The above research studied the influence of tool errors and other geometric errors on machining accuracy, most of the existing comprehensive error models are introduced with geometry error of machine tool, thermal error and cutting force deflection error. In a multi-layer flank milling process, the tool rotation profile error may lead to inter-layer machining interference. However, there has no calculation and analysis of interference in multi-layer machining in machining accuracy prediction at present, it is necessary to establish a new error prediction model to predict the machining accuracy

for this machining method.

In this paper, a new comprehensive error prediction model is proposed based on a multi-layer flank milling process especially for cutting soft work material such as aluminum alloy. The new model incorporates the existing prediction model[45] established by considering the effects of geometric errors of machine tool, workpiece locating errors and spindle thermal deflection errors. This new model considers the effect of inter-layer interference caused by the geometric error of tool rotation profile in machining. Therefore, the prediction accuracy of the new model is higher than that of the existing model, which provides a reference for tool error compensation.

The structure of this paper is as follows. Section 2 analyses the tool error, Section 3 constructs a new comprehensive error prediction model. Section 4 evaluates the prediction model through a machining experiment. Finally, the conclusions are drawn in section 5.

2. Tool error analysis

In this study, material with lower stiffness such as aluminum alloy is selected as work material, thus the effects of tool deflection and wear can be ignored because they are relatively small. Only the tool radial dimension error and setup error are considered, therefore, the tool rotation profile error not affected by the material properties of tool-workpiece and machining parameters.

For an integral end milling tool (as shown in Fig. 3), the definition of the error parameters of tool rotation profile error are listed in Table 1.

Table 1 Definition of tool error factors

Error factors	Error description	Error parameters
Tool radial dimension error	Radius error of cutting edge caused by tool manufacturing or grinding	Deviation between measured values and ideal values for series of tool rotation radius along tool axis
Tool setup error	The clearance between tool holder and tool post, the misalignment between tool axis and spindle axis, which will lead to tool radial runout	

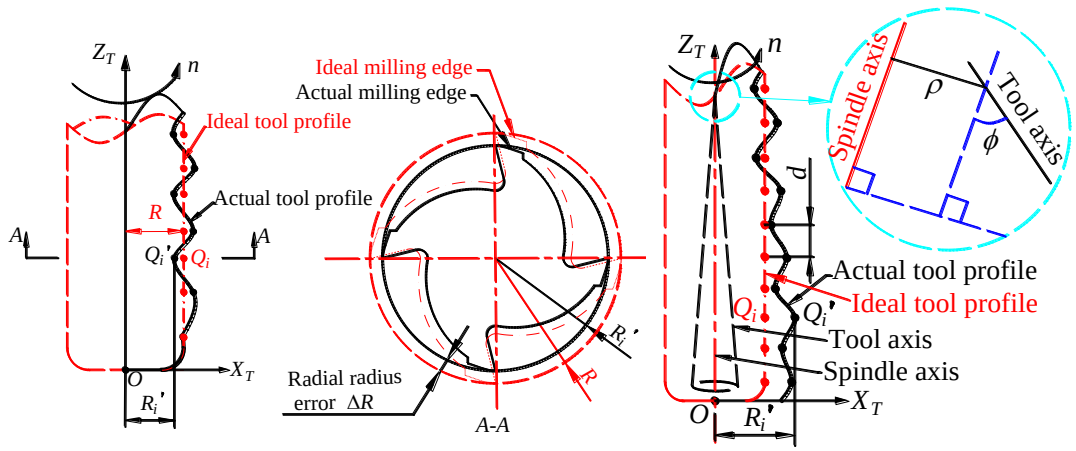

(a) Rotation profile with dimension errors (b) Actual rotation profile with dimension errors and setup errors

Fig. 3 Geometric error of tool rotation profile

The ideal radius of the tool is assumed to be R, as shown in Fig. 3(a), so the ideal envelope formed by tool rotating should be a cylinder with a radius R in machining. Under the influence of tool dimension error, the radius of revolving body along the tool axial are a series of constantly changing values, as shown in Fig. 3(a). The tool setup error contains parallel axis error ρ and inclination angle error ϕ between the tool rotation axis and the spindle rotation axis, as shown in Fig. 3(b). In the case of integrated dimension error and setup error, the radius of the axial section of the actual tool revolving body is constantly changing (as shown in Fig. 3(b)).

As shown in Fig. 3, a radius measuring coordinate system X_TOZ_T for tool revolving body is established, a series of measuring points $Q'_i(i=1,2\cdots,n)$ are selected to measure the radius of revolving body, and its corresponding radius is R'_i. If there is no tool error, the ideal measuring points is Q_i, and its corresponding radius is R. The distance between two adjacent measuring points is d, where n=int(L/d) (int() is the rounding function), and L is the effective length of cutting edge. Therefore, the geometric error of tool rotation profile can be described by R'_i.

In flank milling process, a swept surface is formed by the contact line between the tool envelope and workpiece when the tool moves, so the contact line is an important reference to reflect the profile of a machined surface. The mathematics of flank milling is as follows:

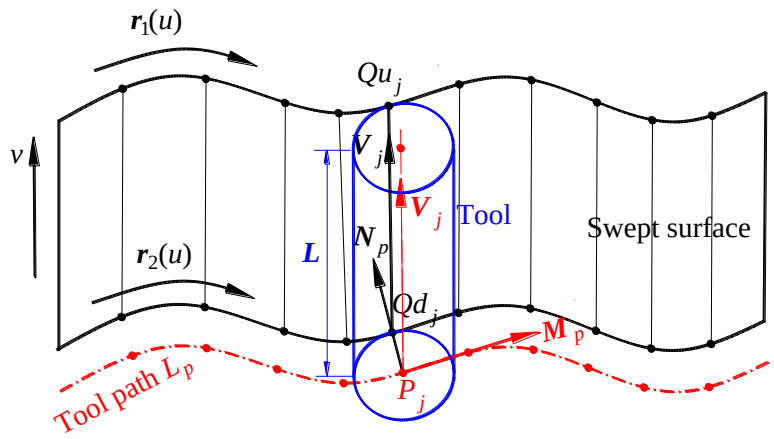

Fig. 4 Motion of tool along tool path

The tool path curve L_p is determined by tool location points P_j (j=1,2,⋯,m), as shown in Fig. 4, the coordinates of tool contact point Qd_j corresponding to P_j is calculated by eq. (1):

$$\boldsymbol{Q}d_j=\boldsymbol{P}_j+R\cdot\boldsymbol{N}_p \tag{1}$$

Where $\boldsymbol{P}_j$ represents the coordinates at P_j, $\boldsymbol{N}_p$ is normal unit vector at P_j.

The top point Qu_j corresponding to Qd_j can be calculated by eq. (2):

$$\boldsymbol{Q}u_j=\boldsymbol{Q}d_j+L\cdot\boldsymbol{V}_j \tag{2}$$

Where $\boldsymbol{V}_j$ is tool orientation vector at P_j.

Therefore, Qd_j and Qu_j can be regarded as a series of interpolation points on bottom guiding curve $\boldsymbol{r}_2(u)$ and top guiding curve $\boldsymbol{r}_1(u)$ at the swept surface respectively, $\boldsymbol{r}_1(u)$ and $\boldsymbol{r}_2(u)$ can be obtained from Qu_j and Qd_j through NURBS curve fitting respectively.

The parametric equation of the swept surface is:

$$\boldsymbol{S}(u,v)=(1-v)\boldsymbol{r}_2(u)+v\boldsymbol{r}_1(u) \qquad u\in[0,1],\ v\in[0,1] \tag{3}$$

The geometric error of tool rotation profile will affect the shape of contact line, thereby affecting the swept surface and machining accuracy. The ideal and actual contact lines can be constructed by ideal points Q_i and the corresponding actual measuring points Q'_i separately. In the sweeping process, the actual tool contact points corresponding to the measuring points can be calculated, so the profile of machining surface can be obtained according to these points.

Note that both geometrical errors of the machine tool and the tool rotation profile error have important influence on the machining surface. However, the geometric errors of machine tool only cause the deviation of tool location and tool orientation, which will

lead to a tool path error. The tool rotation profile error only affects the shape of contact line between tool and workpiece, thus affect the surface accuracy.

3. Comprehensive error modeling

The new model includes the calculation of series of tool contact points on the swept surface in single layer, and the judgment and computation for inter-layer interference.

3.1. Series of tool contact points calculation in single layer

3.1.1. Tool location and orientation calculation

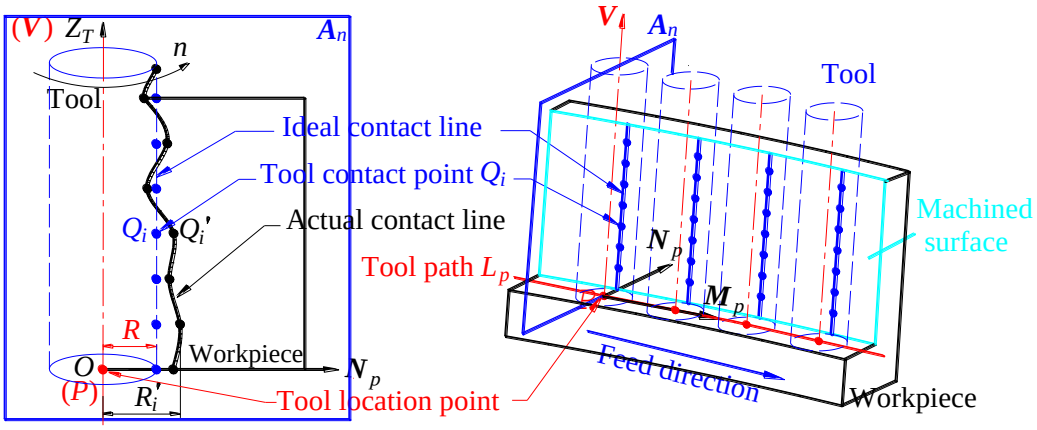

Fig. 5 Sketch of flank milling

As shown in Fig. 5, the tool location points and tool orientation are two important parameters to describe the tool trajectory. The tool moves along the trajectory curve L_p given by the CL-File, the ideal tool tip coordinate X_j, Y_j, Z_j and rotation angle A_j, B_j, C_j can be obtained directly by CL-File, the tool orientation is determined by the direction of its rotation axis. Suppose that the coordinates of an ideal tool location point P on L_p in the workpiece coordinate system(WCS) is $\boldsymbol{P}= (p_x, p_y, p_z)^{\mathrm{T}}$, the tool orientation vector is $\boldsymbol{V}=(v_x, v_y, v_z)^{\mathrm{T}}$. The tool location and tool orientation deviated from the ideal position due to the geometric errors of machine tool, workpiece location errors and spindle thermal deflection errors, so suppose that the actual tool location point corresponding to P is P', and the coordinates of P' in WCS is $\boldsymbol{p}'=(P'_x, P'_y, P'_z)^{\mathrm{T}}$, the tool orientation vector at P' is $\boldsymbol{V}'=(v'_x, v'_y, v'_z)^{\mathrm{T}}$, $\boldsymbol{p}'$ and $\boldsymbol{V}'$ can be calculated by the method of multi-body kinematics and homogeneous transfer matrix with the parameters of the machine tool geometric errors, workpiece location errors and spindle thermal deflection errors (Appendix 2 gives details).

In the same way, the actual tool location point and tool orientation corresponding to each ideal tool location point on L_p can be calculated considering the geometric errors of machine tool, workpiece location errors and spindle thermal deflection errors.

3.1.2. Tool contact points calculation

In reference[46], the calculation method of tool contact points on the swept surface considering the tool runout and tool path errors is given. In this paper, the calculation process of tool contact point is also established with reference to this method. In the machining process, as shown in Fig. 5. At tool location point P: a normal plane $\boldsymbol{A}_n$ is formed by $\boldsymbol{V}$ along the tool axis and normal unit vector $\boldsymbol{N}_p$ of tool trajectory curve L_p at P. The contact line between $\boldsymbol{A}_n$ and tool revolving body is formed, a series of points Q_i are selected as tool contact points on the contact line, and these points corresponding to the measuring points of rotation radius. The calculation process for series of ideal tool contact points Q_i at P and actual tool contact points Q'_i at P' is computed as follows:

(1) Normal vector calculation

It is necessary to calculate the normal vector at tool location point for determining tool contact points. The normal vector at a tool location point is determined by the tangent vector and tool orientation vector, so the tangent vector should be computed firstly. In a multi-axis high-speed machining system, a large number of interpolation points are distributed near each tool location point[47], therefore, the tangent vector at point P can be determined by the interpolation point q_k closest to the point P and the next adjacent interpolation point q_{k+1}. So the tangent vector $\boldsymbol{M}_p$ at P and tangent vector $\boldsymbol{M}'_p$ at P' can be obtained by eq. (4) and eq. (5) respectively:

$$\boldsymbol{M}_p=(M_{px}, M_{py}, M_{pz})^{\mathrm{T}}=(q_{x+1}-q_x, q_{y+1}-q_y, q_{z+1}-q_z)^{\mathrm{T}} \tag{4}$$

$$\boldsymbol{M}'_p =(M'_{px}, M'_{py}, M'_{pz})^{\mathrm{T}}=(q'_{x+1}-q'_x, q'_{y+1}-q'_y, q'_{z+1}-q'_z)^{\mathrm{T}} \tag{5}$$

Where (q_x, q_y, q_z) represents the coordinates of interpolation point q closest to point P, $(q_{x+1}, q_{y+1}, q_{z+1})$ represents the coordinates of interpolation point adjacent to point q, (q'_x, q'_y, q'_z) represents the coordinates of interpolation point q' closest to point P', $(q'_{x+1}, q'_{y+1}, q'_{z+1})$ represents the coordinates of interpolation point adjacent to point q'.

After calculating the tangent vectors, the normal unit vector $\boldsymbol{N}_p$ at P and the normal unit vector $\boldsymbol{N}'_p$ at P' can be calculated by eq. (6) and eq. (7) respectively:

$$\boldsymbol{N}_p = (N_{px}, N_{py}, N_{pz})^{\mathrm{T}} = \frac{\boldsymbol{V} \times \boldsymbol{M}_p}{\left| \boldsymbol{V} \times \boldsymbol{M}_p \right|} \tag{6}$$

$$\boldsymbol{N}'_p = (N'_{px}, N'_{py}, N'_{pz})^{\mathrm{T}} = \frac{\boldsymbol{V}' \times \boldsymbol{M}'_p}{\left| \boldsymbol{V}' \times \boldsymbol{M}'_p \right|} \tag{7}$$

(2) Series of ideal tool contact points Q_i calculation

As shown in Fig. 5, the ideal contact line is parallel to the tool axis and the pitch is the ideal tool radius R without considering any errors. Define a matrix as formula (8):

$$\boldsymbol{E} = [d, 2d, 3d, \cdots, nd] \tag{8}$$

Therefore, the coordinates of Q_i can be obtained by shifting R along the direction of $\boldsymbol{N}_p$ at P and then moving the corresponding distance along the tool orientation, as shown in eq. (9):

$$\begin{aligned} \boldsymbol{Q}_i &= (\boldsymbol{Q}_1, \boldsymbol{Q}_2, \cdots \boldsymbol{Q}_n)^{\mathrm{T}} \\ &= [\boldsymbol{P}, \boldsymbol{P}, \cdots \boldsymbol{P}]^{\mathrm{T}} + R[\boldsymbol{N}_p, \boldsymbol{N}_p, \cdots \boldsymbol{N}_p]^{\mathrm{T}} + (\boldsymbol{V} \cdot \boldsymbol{E})^{\mathrm{T}} \\ &= \begin{bmatrix} P_x + R \cdot N_{px} + d \cdot v_x & P_y + R \cdot N_{py} + d \cdot v_y & P_z + R \cdot N_{pz} + d \cdot v_z \\ P_x + R \cdot N_{px} + 2d \cdot v_x & P_y + R \cdot N_{py} + 2d \cdot v_y & P_z + R \cdot N_{pz} + 2d \cdot v_z \\ \mathrm{M} & \mathrm{M} & \mathrm{M} \\ P_x + R \cdot N_{px} + nd \cdot v_x & P_y + R \cdot N_{py} + nd \cdot v_y & P_z + R \cdot N_{pz} + nd \cdot v_z \end{bmatrix} \end{aligned} \tag{9}$$

(3) Series of actual tool contact points Q'_i calculation

The coordinates of a series of actual tool contact points Q'_i corresponding to P' can be calculated considering all the errors mentioned above, as shown in eq. (10):

$$\begin{aligned} \boldsymbol{Q}'_i &= (\boldsymbol{Q}'_1, \boldsymbol{Q}'_2, \cdots \boldsymbol{Q}'_n)^{\mathrm{T}} \\ &= [\boldsymbol{P}', \boldsymbol{P}', \cdots \boldsymbol{P}']^{\mathrm{T}} + [\boldsymbol{N}'_p \cdot \boldsymbol{R}']^{\mathrm{T}} + (\boldsymbol{V}' \cdot \boldsymbol{E})^{\mathrm{T}} \\ &= \begin{bmatrix} P'_x + R'_1 \cdot N'_{px} + d \cdot v'_x & P'_y + R'_1 \cdot N'_{py} + d \cdot v'_y & P'_z + R'_1 \cdot N'_{pz} + d \cdot v'_z \\ P'_x + R'_2 \cdot N'_{px} + 2d \cdot v'_x & P'_y + R'_2 \cdot N'_{py} + 2d \cdot v'_y & P'_z + R'_2 \cdot N'_{pz} + 2d \cdot v'_z \\ \mathrm{M} & \mathrm{M} & \mathrm{M} \\ P'_x + R'_n \cdot N'_{px} + nd \cdot v'_x & P'_y + R'_n \cdot N'_{py} + nd \cdot v'_y & P'_z + R'_n \cdot N'_{pz} + nd \cdot v'_z \end{bmatrix} \end{aligned} \tag{10}$$

Where $\boldsymbol{R}' = [R'_1 \; R'_2 \; \cdots R'_n]$ represents the tool radius considering tool errors.

According to the above calculation process, the coordinates of series of tool contact points corresponding to each tool location point can be calculated. At last, the tool contact points on swept surface for single layer can be obtained.

3.2. Interference detection and calculation

In multi-layer milling, the row spacing of tool contact points along tool axis is consistent on each sweep surface, so the number of rows of tool contact points on the latter swept surface is more than that on the former swept surface, as shown in Fig. 6.

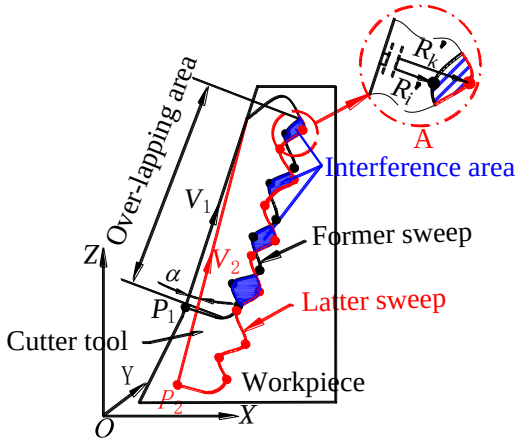

Fig. 6 Illustration of interference

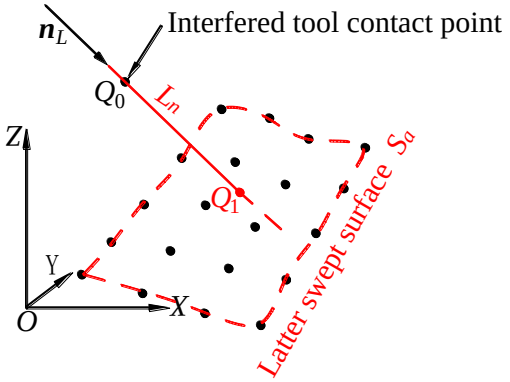

Fig. 7 Position correction for interference tool contact point

The tool partially over-sweeps the machined surface in the former layer when it sweeps in the latter layer, thus the over-lapping area is formed. The swept surface of each layer is covered by the latter surfaces except the last layer. Because of the influence of principle error in tool path planning and geometric error of machine tool, the tool position and tool orientation are deviated in different layers (for example, there may be an included angle α between tool axis vectors in different layers). In the overlap area A of Fig. 6, due to the geometric error of tool rotation profile, the rotation radius R'_k corresponding to the latter tool contact point is larger than the rotation radius R'_i corresponding to the former tool contact point, the undercut interference to the former tool contact points will happen.

In order to obtain the tool contact points on the final machined surface, not only the tool contact points on the single swept surface should be calculated, but also the possible interference effect caused by the sweeping in the latter layers on the tool contact points of the former swept surface should be considered. Analyzing the interference in different situations is necessary because of the change of the tool position and the blank position in the machining process. Take the cutting form in Fig. 6 as an example, the interference effect of the swept surface S_a on the tool contact point

Q_0 in the former layer is analyzed, as shown in Fig. 7. The specific process of interference detection and calculation is as follows:

(1) Parameter equation for single swept surface construction

The tool contact points of each layer are used as measured points, and the 3rd-degree NURBS surface fitting method is used to establish a parameter equation[48]:

$$\boldsymbol{S}(u,v)=\frac{\sum_{i=0}^{m}\sum_{j=0}^{n}B_{i,3}(u)B_{j,3}(v)w_{i,j}\boldsymbol{C}_{i,j}}{\sum_{i=0}^{m}\sum_{j=0}^{n}B_{i,3}(u)B_{j,3}(v)w_{i,j}} \tag{11}$$

Where $\boldsymbol{C}_{i,j}$ is the control point, $w_{i,j}$ is the weight, and $B_{i,3}(u)$, $B_{j,3}(v)$ are B-spline basis functions.

(2) Normal line equation at point Q_0 construction

The normal unit vector formula at point Q_0 on the parameter surface $\boldsymbol{S}(u,v)$ is calculated as follows[48]:

$$\boldsymbol{n}_L(u_0, v_0)=(x_n, y_n, z_n)=\frac{\boldsymbol{S}_u(u_0,v_0)\times\boldsymbol{S}_v(u_0,v_0)}{\left|\boldsymbol{S}_u(u_0,v_0)\times\boldsymbol{S}_v(u_0,v_0)\right|} \tag{12}$$

Where $\boldsymbol{n}_L$ is the normal unit vector at Q_0, $\boldsymbol{S}_u$, $\boldsymbol{S}_v$ are the derivatives of the surface along u and v directions respectively.

The normal line equation at Q_0 is constructed by eq. (13):

$$\boldsymbol{L}_n(t)=\boldsymbol{Q}_0+t\cdot\boldsymbol{n}_L \tag{13}$$

(3) Intersection point Q_1 of $\boldsymbol{L}_n(t)$ and S_a solving

A new space coordinate system has been set up with the normal line as the Z axis, in this coordinate system, the coordinate transformation of the control point $\boldsymbol{C}_{i,j}$ of the NURBS surface is carried out[49], and the equations (14) are established by simultaneous eq. (11):

$$\begin{cases}\boldsymbol{S}'_x(u,v)=\sum_{i=0}^{m}\sum_{j=0}^{n}B_{i,3}(u)B_{j,3}(v)\boldsymbol{C}'_{xij}=0\\ \boldsymbol{S}'_y(u,v)=\sum_{i=0}^{m}\sum_{j=0}^{n}B_{i,3}(u)B_{j,3}(v)\boldsymbol{C}'_{yij}=0\end{cases} \tag{14}$$

Where $\boldsymbol{C}'_{i,j}$ is the control point after transformed.

Equations (14) is solved by using the method of quasi-Newton iterative optimization,

the normal projection point $Q_1(x_1, y_1, z_1)$ of the former tool contact point $Q_0(x_0, y_0, z_0)$ on the latter swept surface thus can be obtained.

(4) Determine whether the latter swept surface S_a produces interference to the former tool contact point P_0

If $Z_0 > Z_1$, the latter swept surface S_a will interfere with Q_0, and replace Q_0 with Q_1 as the updated tool contact point; If $Z_0 \leqslant Z_1$, surface S_a has no effect on Q_0.

All the swept surfaces and tool contact points are traversed by using the interference detection and calculation method, and finally the distribution of tool contact points on the final machined surface can be obtained.

The calculation flow of comprehensive error prediction model for five-axis multi-layer flank milling is shown in Fig. 8.

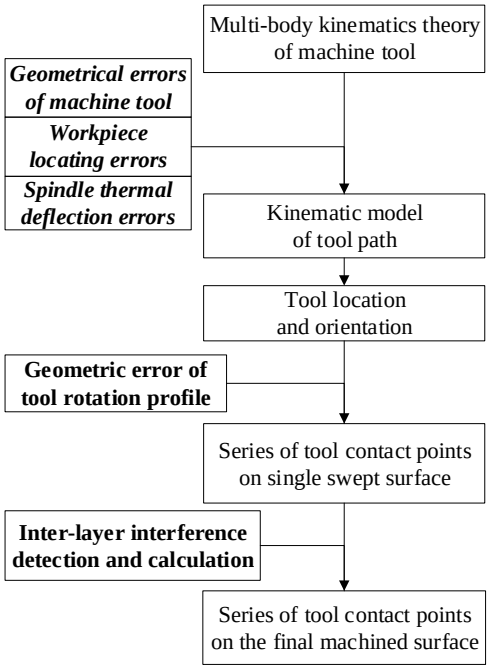

Fig. 8 Calculation flow of comprehensive error prediction model

4. Verification of comprehensive error prediction model

In order to verify the effectiveness of the comprehensive error prediction model, a cutting test was conducted by cutting a workpiece like the letter S which thickness is 3 mm and the milling depth is 45 mm, as shown in Fig. 9. S part is a test piece specially used for five-axis machining, which has ISO standard (ISO 10791-7) and designed by AVIC Chengdu Aircraft Industrial. It has a variable twist angle and its boundary curves have a different curvature, thus S part has a non-developable rule surface and the

position of cutting tool changes from close angle to open angle, the parameters of S part described in reference [50]. Therefore, it can only be machined by five-axis machine tool.

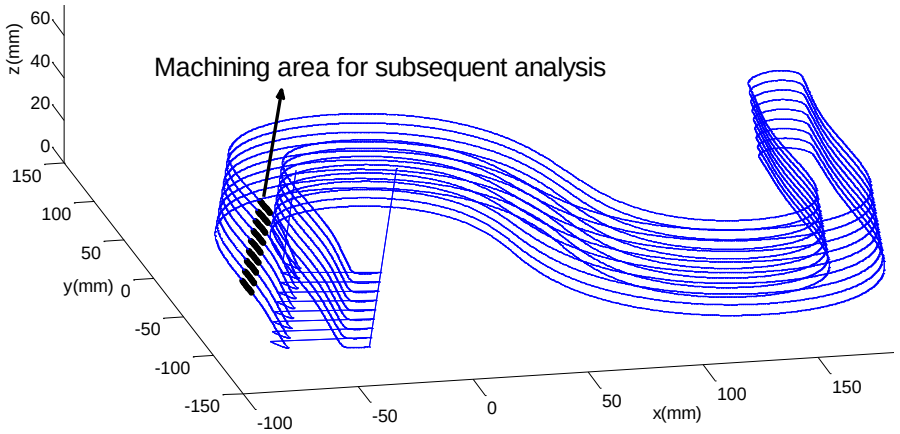

Fig. 9 Tool path of the experiment part

In order to reduce the deflection and the milling force as the wall of the workpiece is very thin, the surface is divided into 9 layers along the tool axial direction. A five-axis machine tool with XFYZBA structure (model GMC820u, CNC system SIEMENS 840D, the details of structure see Appendix 2) is adopted, an integral end milling tool (model Φ20*50*120, as shown in Fig. 10) is selected as cutting tool, aluminum alloy 6061 is selected as work material. Renishaw laser tool measuring system (model NC4) is selected as measuring instrument for tool rotation radius, the measurement results can be accurate to 0.001 mm, so the tool error can be accurately obtained for theoretical calculation. The machining parameters are: spindle speed n=2500 r/min, feed rate V_f=1000 mm/min, radial cutting depth a_e=1 mm.

Fig. 10 Cutting tool

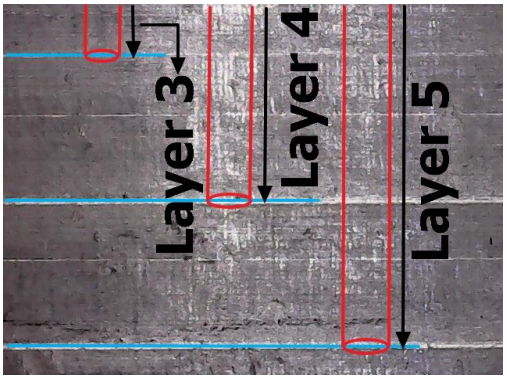

Fig. 11 Final machined surface

The calculation process for comprehensive error model is as follows.

4.1. Error parameters measurement and identification

(1) Tool path error parameters

The 33 geometric error parameters of machine tool can be measured by laser interferometer and identified by the method proposed in reference [51]. The 6 geometric error parameters of workpiece location can be identified by the method proposed in reference [52]. The 5 geometric error parameters of spindle thermal deflection can be identified by the method proposed in reference [45]. All the error parameter values see reference [45].

(2) Tool rotation profile error parameters

The tool is mounted on the spindle and rotates with the spindle, the ideal tool rotation radius R=10 mm. The laser tool measuring system was installed, the distance between two adjacent measuring points is d=3 mm. The tool moves downward along Z axis with a distance of d, a few seconds to stay and the rotation radius is measured. There are 15 measurement points in total, the measurement result is listed in Table 2.

Table 2 Measurement values of geometric error of tool rotation profile

Measuring point i (Direction along the tool tip to hilt)	Z_T (mm)	Measuring radius R'_i (mm)
1	3	10.022
2	6	10.019
3	9	10.020
4	12	10.016
5	15	10.014
6	18	10.012
7	21	10.011
8	24	10.009
9	27	10.005
10	30	10.003
11	33	10.002
12	36	10.001
13	39	9.998
14	42	9.999
15	45	9.995

4.2. Calculation of tool contact points on surface

(1) Calculation of tool contact points on the swept surface in each layer

The distribution of row number for tool contact points in each sweep layer is shown

in Fig. 12. When the tool moves along the direction marked in the figure according to tool path, a series of tool contact points are left on the surface along the direction of tool axis at each tool location point, and the distance between adjacent tool contact point lines in the axial direction fixed d=3 mm. The surface is machined by 9 layers, it can be seen that the first layer has two rows of tool contact points, the second layer has three rows of tool contact points,……, the ninth layer has fifteen rows of tool contact points. The number of tool contact point lines in each layer is marked by the number on the tool contour line in the figure, and the tool contact points in different layers are marked with different colors.

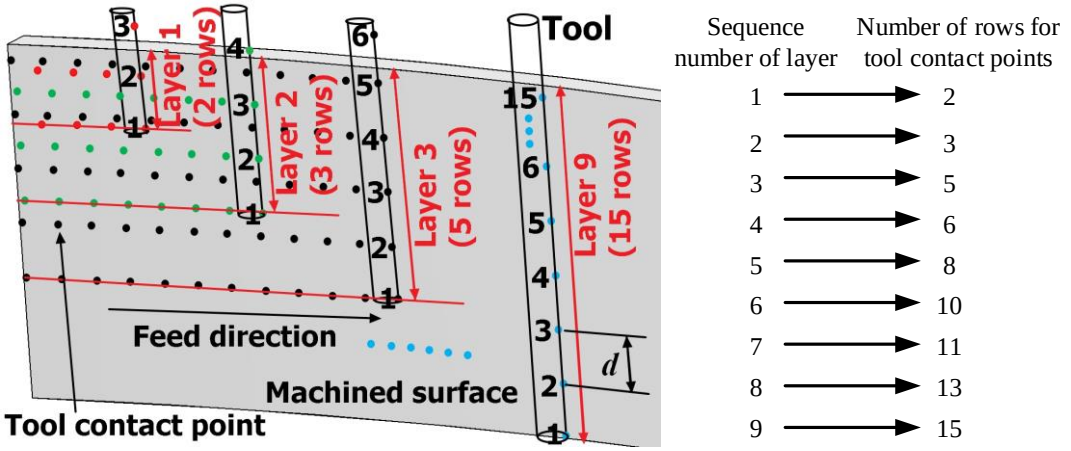

Fig. 12 The distribution of row number for tool contact points in each layer

After obtaining all of error parameters, the distribution of ideal and actual tool contact points on the swept surface in each layer can be calculated respectively by the prediction model according to CL-File. The ideal tool contact points can be calculated by eq. (9) without considering any error, the actual tool contact points can be calculated by eq. (10) introducing both tool path error parameter values and tool rotation profile error parameter values obtained in Section 4.1.

(2) Calculation of tool contact points on the final machined surface

For the actual tool contact points in each layer, the interference analysis was carried out by using the interference detection and calculation method, Table 3 shows the comparison of the coordinates of some points before and after interference on the swept surface in the first layer.

Table 3 Comparison of the coordinate values of some points before and after

interference in the first layer

Point	Coordinates before interference（mm）			Coordinates after interference（mm）		
	X	*Y*	*Z*	*X*	*Y*	*Z*
1	-47.6707	-33.9565	40.9743	-47.6679	-33.9525	40.9772
2	-47.6776	-33.1937	40.9746	-47.6741	-33.1956	40.9785
3	-47.6855	-32.4856	40.9747	-47.6838	-32.4816	40.9756
4	-47.6986	-31.5401	40.9748	-47.6925	-31.5481	40.9775
5	-47.7117	-30.7167	40.9743	-47.7095	-30.7147	40.9728
6	-47.7248	-29.9549	40.9735	-47.7283	-29.9519	40.9722
7	-47.7379	-29.2469	40.9745	-47.7355	-29.2419	40.9724
8	-47.7582	-28.2992	40.9740	-47.7513	-28.2982	40.9796
9	-47.7774	-27.4782	40.9733	-47.7741	-27.4721	40.9788
10	-47.7957	-26.7101	40.9739	-47.7971	-26.7151	40.9775
11	-47.8140	-26.0093	40.9740	-47.8151	-26.0082	40.9779
12	-47.8404	-25.0609	40.9735	-47.8380	-25.0639	40.9712
13	-47.8648	-24.2315	40.9735	-47.8638	-24.2374	40.9741
14	-47.8882	-23.4705	40.9732	-47.8840	-23.4775	40.9787
15	-47.9106	-22.7699	40.9731	-47.9047	-22.7658	40.9737
16	-47.9422	-21.8249	40.9721	-47.9340	-21.8227	40.9745
17	-47.9706	-20.9988	40.9714	-47.9646	-20.9958	40.9782
18	-47.9972	-20.2311	40.9725	-47.9951	-20.2360	40.9743
19	-48.0227	-19.5317	40.9728	-48.0278	-19.5386	40.9744
20	-48.0583	-18.5864	40.9716	-48.0441	-18.5880	40.9653

At last, a series of actual tool contact points on the final machined surface can be obtained after interference detection and calculation. Take the machining area marked in Fig. 9 as an example, the distribution of ideal and actual points in all nine layers on the final machined surface is shown in Fig. 13.

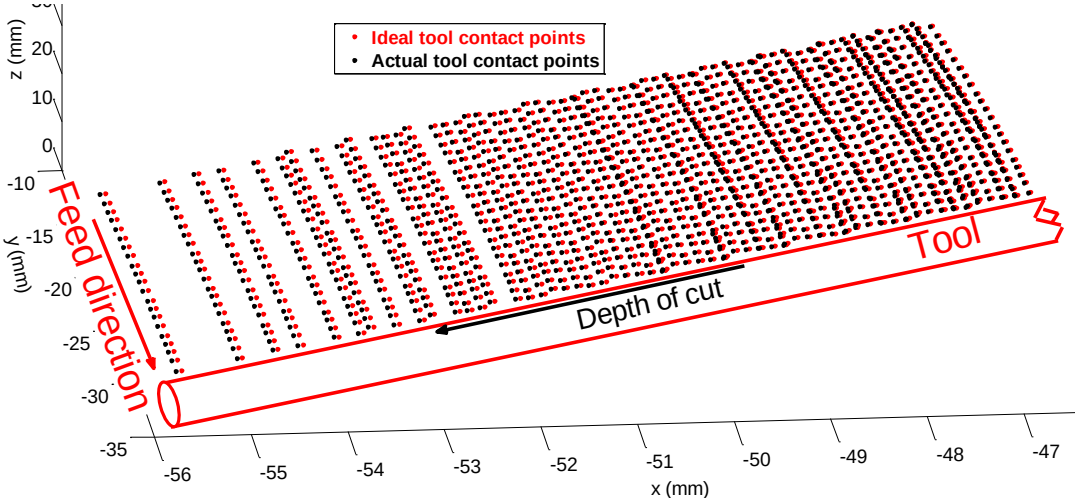

Fig. 13 Distribution of some tool contact points on the final machined surface

Combined with Fig. 12 and Fig. 13, it can be seen that as the latter layer covers the

former layer, the points near the former layer are very dense, and the points near the latter layer are relatively sparse. It can be seen that there is deviation between the ideal tool contact points and the corresponding actual tool contact points, so that the change of tool rotation radius has a certain influence on the position of tool contact points. Of course, the normal machining error can be calculated according to the position of ideal and actual points, see 4.3 for details.

4.3. Verification of surface machining accuracy

The distribution of ideal and actual tool contact points calculated by the model on the final machined surface reflect the shape information of the machined surface, and the normal machining error[26] for each actual tool contact point can be calculated to evaluate the machining error[45].

The normal machining error was calculated by selecting 15 tool contact points on the machined surfaces, Table 4 gives the information of measuring points.

Table 4 Information of measuring tool contact points

Number	Coordinates of points /(mm)			Normal vector /(mm)			Tool position Z_T /(mm)	Layer number
	X	Y	Z	X	Y	Z		
1	-48.3108	-17.8297	39.8569	0.9785	0.0086	-0.2058	21	5
2	-47.9128	-33.7574	39.8280	0.9788	0.0200	-0.2036	21	5
3	-49.5071	-17.1450	34.0174	0.9795	0.0249	-0.1995	18	5
4	-49.1472	-33.2040	33.9825	0.9799	0.0227	-0.1981	18	5
5	-48.5483	-17.8880	38.6620	0.9785	0.0070	-0.2059	15	4
6	-48.1619	-33.9292	38.6389	0.9790	0.0163	-0.2032	15	4
7	-47.9497	-18.2295	41.5817	0.9788	0.0124	-0.2044	18	4
8	-49.1469	-17.5466	35.7422	0.9793	0.0151	-0.2018	12	4
9	-48.7791	-33.6537	35.7160	0.9786	0.0086	-0.2055	12	4
10	-	-	29.3727	0.9795	0.0158	-0.2003	15	6

	50.4499	16.9001						
11	-50.1289	-32.9747	29.3249	0.9791	0.0142	-0.2030	15	6
12	-50.7034	-16.4603	28.1779	0.9796	0.0134	-0.2003	9	5
13	-49.5071	-17.1450	34.0174	0.9785	0.0068	-0.2059	15	5
14	-51.6473	-16.2175	23.5332	0.9794	0.0128	-0.2013	9	6
15	-51.3634	-32.4231	23.4793	0.9788	0.0097	-0.2041	9	6

In order to verify the effects of geometric error of tool rotation profile and inter-layer interference on machining accuracy, three groups of prediction data have been calculated in the theoretical calculation. In the first group, the error prediction values is calculated by the new model considering all errors (as No.2 curve shown in Fig. 14). In the second group, the error prediction values is calculated by the new model but without considering interference(as No.3 curve shown in Fig. 14). In the third group, the error prediction values is calculated by the pre-existing prediction model[45], which doesn't consider the geometric error of tool rotation profile (as No.4 curve shown in Fig. 14). Note that in Figure 14, the normal machining errors of 15 points are measured by the coordinate measuring machine, while the measuring points are the ideal tool contact points calculated by the model, and the normal vector of CMM probe at each point can be calculated by equation (12) in Section 3.2. The information of measuring tool contact points is shown in Table 4 in Section 4.3, the prediction values of normal machining can be calculated according to the coordinates of ideal and actual tool contact points, the calculation method can be seen in reference [45].

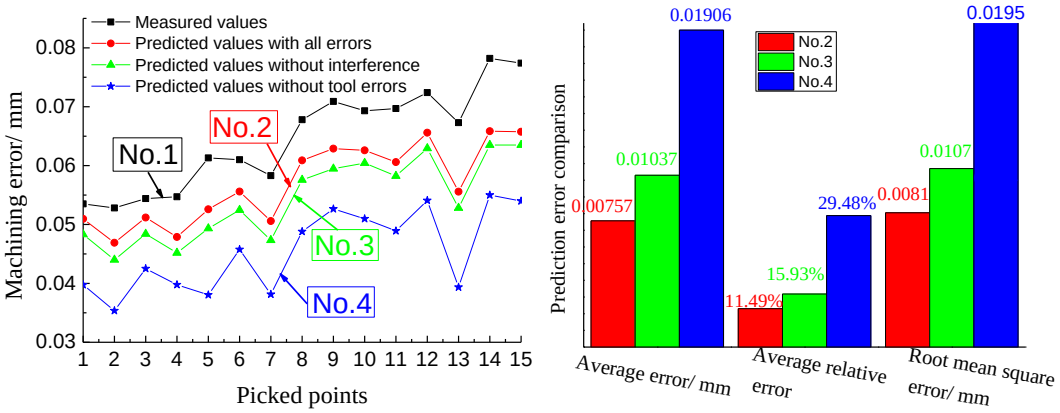

Fig. 14 Comparison of prediction values and measured values

Fig. 15 Prediction error comparison between the three groups of predicted values

The average errors(E_{MAD}), average relative errors(E_{MAP}) and root mean square errors(R_{MES}) of the predicted values for the three groups are used as evaluation standard, as shown in Fig. 15.

Average error:

$$E_{MAD}=\left(\frac{1}{n}\right)\sum_{i=1}^{n}\left|y_i-y_i'\right| \tag{15}$$

Average relative error:

$$E_{MAP}=\left(\frac{1}{n}\right)\sum_{i=1}^{n}\left(\left|y_i-y_i'\right|/\,y_i\right)\times 100\% \tag{16}$$

Root mean square error:

$$R_{MES}=\sqrt{\left(\frac{1}{n}\right)\sum_{i=1}^{n}\left(y_i-y_i'\right)^2} \tag{17}$$

Where y_i is the measured value of machining error, y'_i is the predicted value of machining error.

The following conclusions are obtained by Fig. 14 and Fig. 15:

(1) Compared with the curve No.2, the deviation of the predicted value, the average error and the relative error in No.3 and No.4 are larger, which indicates that the interference caused by tool rotation profile error have certain influence on the machining accuracy.

(2) The variation trend of the four curves is consistent. And by comparing the predicted value of each point in the curves No.2, No.3 and No.4 with the measured values in the curve No.1, it is found that the values of No.2 and No.1 are the closest, and the average error and relative error of predicted values in No.2 are minimum, it is shown that the new comprehensive error model is correct and feasible. Compared with the existing model, the new model has better prediction accuracy.

Comparison and summary of prediction results with existing references

In summary, the calculation and experimental verification for the tool contact points on the machined surface show that the inter-layer interference caused by the geometric

error of tool rotation profile affect the machining accuracy in multi-layer flank milling. However, most of the existing comprehensive error models[8,39-41,44-46] do not consider the inter-layer interference in the study of machining surface accuracy for multi-layer flank milling, and there has no work on calculation and analysis for the possible machining inter-layer interference.

Based on the existing comprehensive error model, a new model established for this machining method is effective, in which the inter-layer interference is taken into consideration. In the experiment, the new prediction model demonstrated higher prediction accuracy by comparing with the prediction results of existing prediction model. Therefore, the model can effectively predict the surface accuracy for multi-layer flank milling, which provides a reference for tool error compensation.

5. Conclusions

(1) In this study, a new comprehensive error prediction model is established for multi-layer flank milling, based on the pre-existing prediction model containing a variety of errors such as geometric errors of machine tool, workpiece locating errors and spindle thermal deflection errors. In the new model, the inter-layer interference is taken into consideration. A series of tool contact points on the final machined surface can be calculated by using the comprehensive error prediction model, so that the subsequent prediction for surface accuracy can be achieved according to these points.

(2) A cutting experiment was carried out to test the effectiveness of the developed model. By comparing the predicted values and measured values of normal machining error for sample points, it shows that the inter-layer interference affects the machining accuracy and the new model has higher prediction accuracy than the existing model. Therefore, the model can effectively predict the surface accuracy for multi-layer flank milling and provides a reference for error compensation.

6. Acknowledgement

This work is supported by the Major Scientific and Technological Innovation Project in Shandong Province (2017CXGC0608-02), China.

7. References

[1] Wang W P, Wang K K. Geometric modeling for swept volume of moving solids[J]. IEEE Computer Graphics and Applications, 1987, 6(12):8-17.

[2] Chu C H, Huang W N, Hsu Y Y. Machining accuracy improvement in five-axis flank milling of ruled surfaces[J]. International Journal of Machine Tools & Manufacture, 2008, 48(7):914-921.

[3] Sprott K, Ravani B. Cylindrical milling of ruled surfaces[J]. International Journal of Advanced Manufacturing Technology, 2008, 38(7-8):649-656.

[4] Hsieh H T, Tsai Y C, Chu C H. Multi-pass progressive tool path planning in five-axis flank milling by particle swarm optimisation[J]. International Journal of Computer Integrated Manufacturing, 2013, 26(10):977-987.

[5] Islam M N, Han U L, Cho D W. Prediction and analysis of size tolerances achievable in peripheral end milling[J]. International Journal of Advanced Manufacturing Technology, 2008, 39(1-2):129-141.

[6] Chu C H, Chen J T. Tool path planning for five-axis flank milling with developable surface approximation[J]. International Journal of Advanced Manufacturing Technology, 2006, 29(7-8):707.

[7] Kim K, Kim M K. Volumetric accuracy analysis based on generalized geometric error model in multi-axis machine tools[J]. Mechanism & Machine Theory, 1991, 26(2):207–219.

[8] Li B, Cao Y, Chen W, et al. Geometry simulation and evaluation of the surface topography in five-axis ball-end milling[J]. International Journal of Advanced Manufacturing Technology, 2017(3):1-17.

[9] Zhang Z, Cai L, Cheng Q, et al. A geometric error budget method to improve machining accuracy reliability of multi-axis machine tools[J]. Journal of Intelligent Manufacturing, 2017:1-25.

[10] Oliaei S N B, Karpat Y. Influence of tool wear on machining forces and tool deflections during micro milling[J]. International Journal of Advanced Manufacturing Technology, 2016, 84(9-12):1963-1980.

[11] Seo T I, Cho M W. Tool trajectory generation based on tool deflection effects in the flat-end milling process (II) —prediction and compensation of milled surface errors—[J]. KSME International Journal, 1999, 13(12):918-930.

[12] Zheng D X, Wang K Q. Research and realization of line contact rotate-milling[J]. Machinery Design & Manufacture, 2009.

[13] Zeng W, Jiang X, Blunt L. Surface characterization-based tool wear monitoring in peripheral milling[J]. International Journal of Advanced Manufacturing Technology, 2009, 40(3-4):226-233.

[14] Arizmendi, Miguel, Fernandez, et al. Effect of tool setting error on the topography of surfaces machined by peripheral milling[J]. International Journal of Machine Tools & Manufacture, 2009, 49(1):36-52.

[15] Ryu S H, Choi D K, Chu C N. Roughness and texture generation on end milled surfaces[J]. International Journal of Machine Tools & Manufacture, 2006, 46(3):404-412.

[16] Weinert K, Surmann T, Enk D, et al. The effect of runout on the milling tool vibration and surface quality[J]. Production Engineering, 2007, 1(3):265-270.

[17] Guo Q, Sun Y W, Guo D M. Analytical modeling of geometric errors induced by cutter runout and tool path optimization for five-axis flank machining[J]. Science in China Series E: Technological Sciences, 2011, 54(12):3180-3190.

[18] M. Kruger, B. Denkena. Model-based identification of tool runout in end milling and estimation of surface roughness from measured cutting forces[J]. International Journal of Advanced Manufacturing Technology, 2013, 65(5-8):1067-1080.

[19] Artetxe E, Olvera D, Lacalle L N L D, et al. Solid subtraction model for the surface topography prediction in flank milling of thin-walled integral blade rotors (IBRs)[J]. International Journal of Advanced Manufacturing Technology, 2016:1-12.

[20] Fu Z, Yang W, Wang X, et al. An analytical force model for ball-end milling based on a predictive machining theory considering cutter runout[J]. The International Journal of Advanced Manufacturing Technology, 2016, 84(9-12):2449-2460.

[21] Liu X, Soshi M, Sahasrabudhe A, et al. A geometrical simulation system of ball

end finish milling process and its application for the prediction of surface micro features[J]. Journal of Manufacturing Science & Engineering, 2006, 128(1):74-85.

[22] Sriyotha P, Sahasrabudhe A, Yamazaki K, et al. Geometrical modelling of a ball-end finish milling process for a surface finish[J]. Proceedings of the Institution of Mechanical Engineers Part B Journal of Engineering Manufacture, 2006, 220(4):467-477.

[23] Wan M, Zhang W H, Dang J W, et al. New procedures for calibration of instantaneous cutting force coefficients and cutter runout parameters in peripheral milling[J]. International Journal of Machine Tools & Manufacture, 2009, 49(14):1144-1151.

[24] Qiang G, Sun Y, Guo D. New mathematical method for the determination of cutter runout parameters in flat-end milling[J]. Chinese Journal of Mechanical Engineering, 2012, 25(5):947-952.

[25] Zeroudi N, Fontaine M. Prediction of tool deflection and tool path compensation in ball-end milling[M]. Springer-Verlag New York, Inc. 2015.

[26] Yuan M, Wang X, Jiao L, et al. Prediction of dimension error based on the deflection of cutting tool in micro ball-end milling[J]. International Journal of Advanced Manufacturing Technology, 2017(5):1-13.

[27] Ko J H, Yun W S, Cho D W, et al. Development of a virtual machining system, part 1: approximation of the size effect for cutting force prediction[J]. International Journal of Machine Tools & Manufacture, 2002, 42(15):1595-1605.

[28] Zhang C, Zhang H. Modelling and prediction of tool wear using LS-SVM in milling operation[J]. International Journal of Computer Integrated Manufacturing, 2015, 29(1):1-16.

[29] Guo F W, Chang L, Yin H C, et al. Tool wear monitoring based on cointegration modelling of multisensory information[J]. International Journal of Computer Integrated Manufacturing, 2014, 27(5):9.

[30] Ferreira P M, Liu C R. An analytical quadratic model for the geometric error of a machine tool[J]. Journal of Manufacturing Systems, 1986, 5(1):51-63.

[31] Kiridena V, Ferreira P M. Mapping the effects of positioning errors on the

volumetric accuracy of five-axis CNC machine tools[J]. International Journal of Machine Tools & Manufacture, 1993, 33(3):417-437.

[32] Fan J W, Guan J L, Wang W C, et al. A universal modeling method for enhancement the volumetric accuracy of CNC machine tools [J]. Journal of Materials Processing Technology, 2002, 129(1-3): 624-628.

[33] Zhang Z F, Liu Y W, Liu L B, et al. Thermal error modeling for five-axis NC machine based on multi-body system theory[J]. Journal of Hebei University of Technology, 2000.

[34] Jian Q. Thermal errors of planer type NC machine tools and its improvement measures[J]. Journal of Mechanical Engineering, 2012, 48(21):149.

[35] Liu K, Li T, Wang Y, et al. Physically based modeling method for comprehensive thermally induced errors of CNC machining centers[J]. International Journal of Advanced Manufacturing Technology, 2017(6):1-12.

[36] Kang Y, Rong Y, Yang J A. Computer-aided fixture design verification: Part 1 — the framework and modeling[C]// ASME 2002 International Design Engineering Technical Conferences and Computers and Information in Engineering Conference. 2002:827-835.

[37] Qin G H, Zhang W H, Wan M, et al. A mathematical approach to analysis and optimal design of a fixture locating scheme[J]. The International Journal of Advanced Manufacturing Technology, 2006, 29(3):349-359.

[38] Khodaygan S. Manufacturing error compensation based on cutting tool location correction in machining processes[J]. International Journal of Computer Integrated Manufacturing, 2014, 27(11):10.

[39] Srivastava A K, Veldhuis S C, Elbestawit M A. Modelling geometric and thermal errors in a five-axis CNC machine tool[J]. International Journal of Machine Tools & Manufacture, 1995, 35(9):1321-1337.

[40] Zhang Y, Yang J, Xiang S, et al. Volumetric error modeling and compensation considering thermal effect on five-axis machine tools [J]. Proceedings of the Institution of Mechanical Engineers, Part C, Journal of Mechanical Engineering Science, 2013, 227(5): 1102-1115.

[41] Zhang Z, Liu Z, Cheng Q, et al. An approach of comprehensive error modeling and accuracy allocation for the improvement of reliability and optimization of cost of a multi-axis NC machine tool[J]. International Journal of Advanced Manufacturing Technology, 2016, 89(1-4):1-19.

[42] Liang D J C, Li H F, Yuan J X, et al. A comprehensive error compensation system for correcting geometric, thermal, and cutting force-induced errors[J]. International Journal of Advanced Manufacturing Technology, 1997, 13(10):708-712.

[43] Ramesh R, Mannan M A, Poo A N. Error compensation in machine tools — a review: Part I: geometric, cutting-force induced and fixture-dependent errors[J]. International Journal of Machine Tools & Manufacture, 2000, 40(9):1235-1256.

[44] Yu H Z, Qin S F, Ding G F, et al. Integration of tool error identification and machining accuracy prediction into machining compensation in flank milling [J]. International Journal of Advanced Manufacturing Technology, 2019, 102(9-12): 3121-3134.

[45] Peng L. Research on development of machining precision prediction system for five-axis flank milling[D]. Chengdu: Master Thesis of Southwest Jiaotong University, 2013.

[46] Yu H Z, Qin S F, Ding G F, et al. Development of prediction model for machining precision of five-axis flank milling based on tool runout error[J/OL]. Computer Integrated Manufacturing Systems, 2019, http://kns.cnki.net/kcms/detail/11.5946.tp.20190705.1403.002.html.

[47] Kuznetsov E B, Yakimovich A Y. The best parameterization for parametric interpolation[M]. Elsevier Science Publishers B.V, 2006.

[48] Piegl L, Tiller W. Non-uniform rational B-splines (Version 2)[M]. Peking: Tsinghua University press, 2010.

[49] Wang B Q, Zhang L, Li D S. Rapid calculation of intersection points between NURBS surface and line in reverse engineering[J]. Journal of Engineering Graphics, 2010, 154(2):149-150.

[50] Wang W, Jiang Z, Tao W, et al. A new test part to identify performance of five-axis

machine tool—part I: geometrical and kinematic characteristics of S part[J]. The International Journal of Advanced Manufacturing Technology, 2015, 79(5-8):729-738.

[51] Zhu S W, Ding G F, Qin S F, et al. Integrated geometric error modeling, identification and compensation of CNC machine tools[J]. International Journal of Machine Tools & Manufacture,2012, 52(1):24-29.

[52] Zhu S W, Ding G F, Ma S W, et al. Workpiece locating error prediction and compensation in fixtures[J]. International Journal of Advanced Manufacturing Technology, 2013, 67(5-8):1423-1432.

Appendix 1

Notation

R ideal radius of tool

X_TOZ_T radius measuring coordinate system

Q'_i actual tool contact points

$R_i(i=1,2\cdots\cdots,n)$ series radius of tool rotation profile

Q_i ideal tool contact points

d distance between the measuring points

n the number of measuring points

L the effective length of cutting edge

L_p ideal tool path

P ideal tool location point

$\boldsymbol{P}$ ideal tool location point in WCS

$\boldsymbol{V}$ ideal tool orientation in WCS

P' actual tool location point

$\boldsymbol{p}'$ actual tool location point in WCS

$\boldsymbol{V}'$ actual tool orientation in WCS

X_j, Y_j, Z_j ($j=1,2,\cdots,m$) ideal tool tip in WCS

A_j, B_j, C_j ideal rotation angle around A-axis, B-axis and C-axis

$\boldsymbol{T}'_{ij}$ error feature transformation matrix

$\boldsymbol{P}_t$ ideal tool location point in TCS

$\boldsymbol{T}'_{ij}(r)$ actual feature transformation matrix with rotation error

$\boldsymbol{V}_t$ tool orientation in TCS

$\boldsymbol{A}_p$ swept surface

$\boldsymbol{A}_n$ normal plane

$\boldsymbol{M}'_p$ actual tangent vector

$\boldsymbol{M}_p$ ideal tangent vector

$\boldsymbol{N}_p$ normal vector at P

$\boldsymbol{N}'_p$ normal vector at P'

R_k, R_i radius of tool rotation profile

$\boldsymbol{C}_{i,j}$ control points

$w_{i,j}$ weights

$B_{i,3}(u)$, $B_{j,3}(v)$ B-spline basis functions

$\boldsymbol{n}_L$ normal unit vector

$\boldsymbol{S}_u$, $\boldsymbol{S}_v$ derivatives of the surface along u and v directions

$\boldsymbol{L}_n(t)$ normal line

$\boldsymbol{C}'_{i,j}$ control points after transformation

α angle of between tool axis and spindle axis

Appendix 2

Taking a XFYZBA five-axis machine tool for example, its structure is shown in Fig. 16, the calculation model of tool location and orientation is as follows:

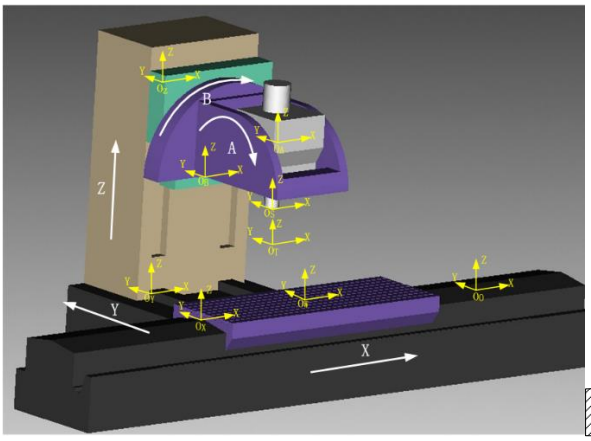

Fig. 16 XFYZBA five-axis machine tool

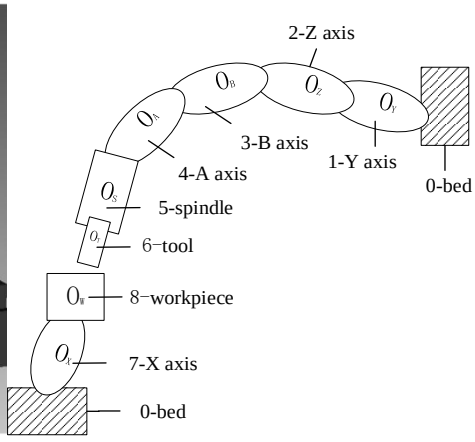

Fig. 17 Topological construction of the process system

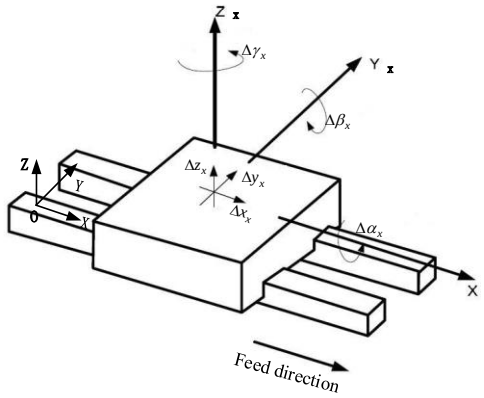

Fig. 18 Geometric error parameters of translational axis

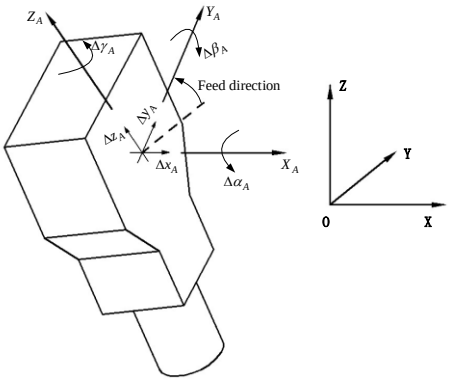

Fig. 19 Geometric error parameters of rotation axis

The geometric error parameters of five-axis machine tool (a total of 33 items) is shown in Table 5.

Table 5 Geometric error parameters of five-axis machine tool

Geometric parameters		Expression	Geometric parameters		Expression
X translational axis	positioning error	Δx_X	Mutual position of translational axis	perpendicularity error for X and Y	$\Delta\gamma_{XY}$
	straightness error with respect to Y	Δy_X			
	straightness error with	Δz_X		perpendicularity error for X and Z	$\Delta\beta_{XZ}$
	roll error	$\Delta\alpha_X$			
	pitch error	$\Delta\beta_X$		perpendicularity error for Y and Z	$\Delta\alpha_{YZ}$
	yaw error	$\Delta\gamma_X$			
Y translational axis	straightness error with respect to X	Δx_Y	A rotation axis	runout error with X	Δx_A
	positioning error	Δy_Y		runout error with Y	Δy_A
	straightness error with	Δz_Y		runout error with Z	Δz_A
	pitch error	$\Delta\alpha_Y$		rotation error around X	$\Delta\alpha_A$
	roll error	$\Delta\beta_Y$		rotation error around Y	$\Delta\beta_A$
	yaw error	$\Delta\gamma_Y$		rotation error around Z	$\Delta\gamma_A$

Geometric parameters		Expression	Geometric parameters		Expression
Z translational axis	straightness error with respect to X	Δx_Z	B rotation axis	runout error with X	Δx_B
	straightness error with	Δy_Z		runout error with Y	Δy_B
	positioning error	Δz_Z		runout error with Z	Δz_B
	pitch error	$\Delta \alpha_Z$		rotation error around X	$\Delta \alpha_B$
	yaw error	$\Delta \beta_Z$		rotation error around Y	$\Delta \beta_B$
	roll error	$\Delta \gamma_Z$		rotation error around Z	$\Delta \gamma_B$

The error parameters of workpiece locating errors and spindle thermal deflection errors are shown in Fig. 20 and Fig. 21. The ideal transformation matrices and error transformation matrices are shown is Table 6.

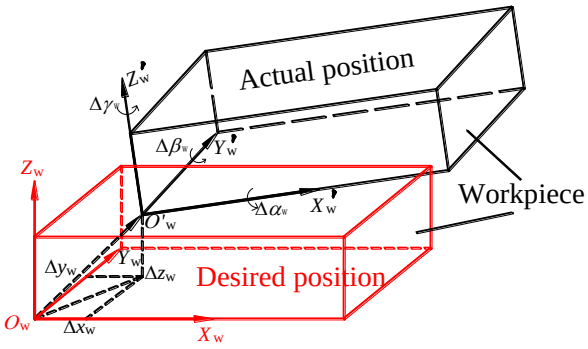

Fig. 20 Parameters of workpiece locating errors

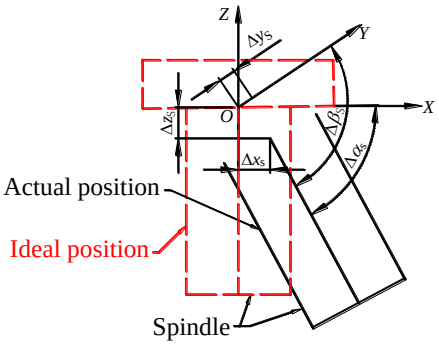

Fig. 21 Parameters of spindle thermal deflection errors

Table 6 Transformation matrices

Adjacent body		Ideal transformation matrix	Error transformation matrix with rotation error	Error transformation matrix
0-1 Y axis	Position transformation	$\boldsymbol{T}_{01p}=\boldsymbol{I}_{4\times4}$	$\boldsymbol{T}'_{01p}(r)=\begin{pmatrix}1 & -\Delta\gamma_{XY} & 0 & 0\\ \Delta\gamma_{XY} & 1 & 0 & 0\\ 0 & 0 & 1 & 0\\ 0 & 0 & 0 & 1\end{pmatrix}$	$\boldsymbol{T}'_{01p}=\begin{pmatrix}1 & -\Delta\gamma_{XY} & 0 & 0\\ \Delta\gamma_{XY} & 1 & 0 & 0\\ 0 & 0 & 1 & 0\\ 0 & 0 & 0 & 1\end{pmatrix}$

	Motion transformation	$\boldsymbol{T}_{01s}=\begin{pmatrix}1&0&0&0\\0&1&0&S_y\\0&0&1&0\\0&0&0&1\end{pmatrix}$	$\boldsymbol{T}'_{01s}(r)=\begin{pmatrix}1&-\Delta\gamma_Y&\Delta\beta_Y&0\\\Delta\gamma_Y&1&-\Delta\alpha_Y&0\\-\Delta\beta_Y&\Delta\alpha_Y&1&0\\0&0&0&1\end{pmatrix}$	$\boldsymbol{T}'_{01s}=\begin{pmatrix}1&-\Delta\gamma_Y&\Delta\beta_Y&\Delta x_Y\\\Delta\gamma_Y&1&-\Delta\alpha_Y&\Delta y_Y\\-\Delta\beta_Y&\Delta\alpha_Y&1&\Delta z_Y\\0&0&0&1\end{pmatrix}$
1-2 Z axis	Position transformation	$\boldsymbol{T}_{12p}=\begin{pmatrix}1&0&0&0\\0&1&0&0\\0&0&1&L_t+L_s\\0&0&0&1\end{pmatrix}$	$\boldsymbol{T}'_{12p}(r)=\begin{pmatrix}1&0&\Delta\beta_{XZ}&0\\0&1&-\Delta\alpha_{YZ}&0\\-\Delta\beta_{XZ}&\Delta\alpha_{YZ}&1&0\\0&0&0&1\end{pmatrix}$	$\boldsymbol{T}'_{12p}=\begin{pmatrix}1&0&\Delta\beta_{XZ}&0\\0&1&-\Delta\alpha_{YZ}&0\\-\Delta\beta_{XZ}&\Delta\alpha_{YZ}&1&0\\0&0&0&1\end{pmatrix}$
	Motion transformation	$\boldsymbol{T}_{12s}=\begin{pmatrix}1&0&0&0\\0&1&0&0\\0&0&1&S_s\\0&0&0&1\end{pmatrix}$	$\boldsymbol{T}'_{12s}(r)=\begin{pmatrix}1&-\Delta\gamma_Z&\Delta\beta_Z&0\\\Delta\gamma_Z&1&-\Delta\alpha_Z&0\\-\Delta\beta_Z&\Delta\alpha_Z&1&0\\0&0&0&1\end{pmatrix}$	$\boldsymbol{T}'_{12s}=\begin{pmatrix}1&-\Delta\gamma_Z&\Delta\beta_Z&\Delta x_Z\\\Delta\gamma_Z&1&-\Delta\alpha_Z&\Delta y_Z\\-\Delta\beta_Z&\Delta\alpha_Z&1&\Delta z_Z\\0&0&0&1\end{pmatrix}$
2-3 B axis	Position transformation	$\boldsymbol{T}_{23p}=\boldsymbol{I}_{4\times4}$	$\boldsymbol{T}'_{23p}(r)=\boldsymbol{I}_{4\times4}$	$\boldsymbol{T}'_{23p}=\boldsymbol{I}_{4\times4}$
	Motion transformation	$\boldsymbol{T}_{23s}=\begin{pmatrix}\cos B&0&\sin B&0\\0&1&0&0\\-\sin B&0&\cos B&0\\0&0&0&1\end{pmatrix}$	$\boldsymbol{T}'_{23s}(r)=\begin{pmatrix}1&-\Delta\gamma_B&\Delta\beta_B&0\\\Delta\gamma_B&1&-\Delta\alpha_B&0\\-\Delta\beta_B&\Delta\alpha_B&1&0\\0&0&0&1\end{pmatrix}$	$\boldsymbol{T}'_{23s}=\begin{pmatrix}1&-\Delta\gamma_B&\Delta\beta_B&\Delta x_B\\\Delta\gamma_B&1&-\Delta\alpha_B&\Delta y_B\\-\Delta\beta_B&\Delta\alpha_B&1&\Delta z_B\\0&0&0&1\end{pmatrix}$
3-4 A axis	Position transformation	$\boldsymbol{T}_{34p}=\boldsymbol{I}_{4\times4}$	$\boldsymbol{T}'_{34p}(r)=\boldsymbol{I}_{4\times4}$	$\boldsymbol{T}'_{34p}=\boldsymbol{I}_{4\times4}$
	Motion transformation	$\boldsymbol{T}_{34s}=\begin{pmatrix}1&0&0&0\\0&\cos A&-\sin A&0\\0&\sin A&\cos A&0\\0&0&0&1\end{pmatrix}$	$\boldsymbol{T}'_{34s}(r)=\begin{pmatrix}1&-\Delta\gamma_A&\Delta\beta_A&0\\\Delta\gamma_A&1&-\Delta\alpha_A&0\\-\Delta\beta_A&\Delta\alpha_A&1&0\\0&0&0&1\end{pmatrix}$	$\boldsymbol{T}'_{34s}=\begin{pmatrix}1&-\Delta\gamma_A&\Delta\beta_A&\Delta x_A\\\Delta\gamma_A&1&-\Delta\alpha_A&\Delta y_A\\-\Delta\beta_A&\Delta\alpha_A&1&\Delta z_A\\0&0&0&1\end{pmatrix}$
4-5 spindle	Position transformation	$\boldsymbol{T}_{45p}=\begin{pmatrix}1&0&0&0\\0&1&0&0\\0&0&1&-L_s\\0&0&0&1\end{pmatrix}$	$\boldsymbol{T}'_{45p}(r)=\begin{pmatrix}1&0&\Delta\beta_S&0\\0&1&-\Delta\alpha_S&0\\-\Delta\beta_S&\Delta\alpha_S&1&0\\0&0&0&1\end{pmatrix}$	$\boldsymbol{T}'_{45p}=\begin{pmatrix}1&0&\Delta\beta_S&\Delta x_S\\0&1&-\Delta\alpha_S&\Delta y_S\\-\Delta\beta_S&\Delta\alpha_S&1&\Delta z_S\\0&0&0&1\end{pmatrix}$
	Motion transformation	$\boldsymbol{T}_{45s}=\boldsymbol{I}_{4\times4}$	$\boldsymbol{T}'_{45s}(r)=\boldsymbol{I}_{4\times4}$	$\boldsymbol{T}'_{45s}=\boldsymbol{I}_{4\times4}$

5-6 tool	Position transformation	$\boldsymbol{T}_{56p}=\begin{pmatrix}1&0&0&0\\0&1&0&0\\0&0&1&-L_t\\0&0&0&1\end{pmatrix}$	$\boldsymbol{T}'_{56p}(r)=\boldsymbol{I}_{4\times4}$	$\boldsymbol{T}'_{56p}=\boldsymbol{I}_{4\times4}$
	Motion transformation	$\boldsymbol{T}_{56s}=\boldsymbol{I}_{4\times4}$	$\boldsymbol{T}'_{56s}(r)=\boldsymbol{I}_{4\times4}$	$\boldsymbol{T}'_{56s}=\boldsymbol{I}_{4\times4}$
0-7 X axis	Position transformation	$\boldsymbol{T}_{07p}=\boldsymbol{I}_{4\times4}$	$\boldsymbol{T}'_{07p}(r)=\boldsymbol{I}_{4\times4}$	$\boldsymbol{T}'_{07p}=\boldsymbol{I}_{4\times4}$
	Motion transformation	$\boldsymbol{T}_{07s}=\begin{pmatrix}1&0&0&-S_x\\0&1&0&0\\0&0&1&0\\0&0&0&1\end{pmatrix}$	$\boldsymbol{T}'_{07s}(r)=\begin{pmatrix}1&-\Delta\gamma_X&\Delta\beta_X&0\\\Delta\gamma_X&1&-\Delta\alpha_X&0\\-\Delta\beta_X&\Delta\alpha_X&1&0\\0&0&0&1\end{pmatrix}$	$\boldsymbol{T}'_{07s}=\begin{pmatrix}1&-\Delta\gamma_X&\Delta\beta_X&\Delta x_X\\\Delta\gamma_X&1&-\Delta\alpha_X&\Delta y_X\\-\Delta\beta_X&\Delta\alpha_X&1&\Delta z_X\\0&0&0&1\end{pmatrix}$
7-8 workpiece	Position transformation	$\boldsymbol{T}_{78p}=\boldsymbol{I}_{4\times4}$	$\boldsymbol{T}'_{78p}(r)=\begin{pmatrix}1&-\Delta\gamma_W&\Delta\beta_W&0\\\Delta\gamma_W&1&-\Delta\alpha_W&0\\-\Delta\beta_W&\Delta\alpha_W&1&0\\0&0&0&1\end{pmatrix}$	$\boldsymbol{T}'_{78p}=\begin{pmatrix}1&-\Delta\gamma_W&\Delta\beta_W&\Delta x_W\\\Delta\gamma_W&1&-\Delta\alpha_W&\Delta y_W\\-\Delta\beta_W&\Delta\alpha_W&1&\Delta z_W\\0&0&0&1\end{pmatrix}$
	Motion transformation	$\boldsymbol{T}_{78s}=\boldsymbol{I}_{4\times4}$	$\boldsymbol{T}'_{78s}(r)=\boldsymbol{I}_{4\times4}$	$\boldsymbol{T}'_{78s}=\boldsymbol{I}_{4\times4}$

The actual tool location point in WCS can be calculated by eq. (18):

$$\begin{aligned}\boldsymbol{P}'=(&\boldsymbol{T}_{07p}\boldsymbol{T}'_{07p}\boldsymbol{T}_{07s}\boldsymbol{T}'_{07s}\boldsymbol{T}_{78p}\boldsymbol{T}'_{78p}\boldsymbol{T}_{78s}\boldsymbol{T}'_{78s})^{-1}\boldsymbol{T}_{01p}\boldsymbol{T}'_{01p}\\&\boldsymbol{T}_{01s}\boldsymbol{T}'_{01s}\boldsymbol{T}_{12p}\boldsymbol{T}'_{12p}\boldsymbol{T}_{12s}\boldsymbol{T}'_{12s}\boldsymbol{T}_{23p}\boldsymbol{T}'_{23p}\boldsymbol{T}_{23s}\boldsymbol{T}'_{23s}\boldsymbol{T}_{34p}\boldsymbol{T}'_{34p}\\&\boldsymbol{T}_{34s}\boldsymbol{T}'_{34s}\boldsymbol{T}_{45p}\boldsymbol{T}'_{45p}\boldsymbol{T}_{45s}\boldsymbol{T}'_{45s}\boldsymbol{T}_{56p}\boldsymbol{T}'_{56p}\boldsymbol{T}_{56s}\boldsymbol{T}'_{56s}\boldsymbol{P}_t\end{aligned}\tag{18}$$

The actual tool orientation in WCS can be calculated by eq. (19):

$$\begin{aligned}\boldsymbol{V}'=(&\boldsymbol{T}'_{07p}(r)\boldsymbol{T}'_{07s}(r)\boldsymbol{T}'_{78p}(r)\boldsymbol{T}'_{78s}(r))^{-1}\boldsymbol{T}'_{01p}(r)\boldsymbol{T}'_{01s}(r)\\&\boldsymbol{T}'_{12p}(r)\boldsymbol{T}'_{12s}(r)\ \boldsymbol{T}'_{23p}(r)\ \boldsymbol{T}_{23s}\boldsymbol{T}'_{23s}(r)\boldsymbol{T}'_{34p}(r)\boldsymbol{T}_{34s}(r)\boldsymbol{T}'_{34s}\\&\boldsymbol{T}'_{45p}(r)\boldsymbol{T}'_{45s}(r)\boldsymbol{T}'_{56p}(r)\boldsymbol{T}'_{56s}(r)\ \boldsymbol{V}_t\end{aligned}\tag{19}$$

The ideal tool orientation in WCS can be calculated by eq. (20):

$$\boldsymbol{V}=\boldsymbol{T}_{23s}\boldsymbol{T}_{34s}\boldsymbol{V}_t\tag{20}$$